Direct Spectroscopic Observation of Hole Polaron in Lead Halide Perovskites

Cunming Liu,[†,&,*] Hsinhan Tsai,[‡] Wanyi Nie,[‡] David Gosztola,[$] Xiaoyi Zhang[†,*]

[†]X-ray Science Division and [$]Center for Nanoscale Materials, Argonne National Laboratory, 9700 S. Cass Avenue, Lemont, IL 60439.

[‡] Center for Integrated Nano Technologies, Los Alamos National Laboratory, Los Alamos, NM 87545.

[&]Current Address: A204 Chemical and Life Science Laboratory, University of Illinois Urbana-Champaign, 600 S. Mathews Ave. Urbana, IL 61801.

*E-mail: lcmingsc@gmail.com; xyzhang@anl.gov.

Abstract

Intrinsic photophysical origin of lead halide perovskites (LHPs) succeeding in optolectronic applications still remains hotly debated. Here, by using the ultrafast X-ray transient absorption spectroscopy, we successfully tracked the fate of photogenerated charge carriers at room temperature within the thin films of two classic LHPs, namely $MAPbBr_3$ (MA: CH_3NH_3) and $FAPbBr_3$ (FA: $CH(NH_2)_2$). We clearly observed in both thin films that the hole polaron is formed by localizing the photogenerated hole at Br 4p orbital and concurrently distorting the local structure surrounding Br atom after the photoexcitation. Furthermore, the bigger cation FA in the cavity of $[PbBr_6]^{4-}$ octahedral framework induces larger hole polaron effect due to its p orbital hybridization into valence and conduction bands, correlating with the slower charge carrier recombination dynamics. Our direct experimental observation of the localized hole polaron in perovskites should advance the fundamental comprehension of charge carrier behavior within LHPs and their related devices.

Table of Contents Graphic

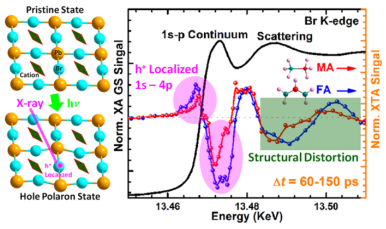

Lead halide perovskites (LHPs) with the formula $APbX_3$ (A = MA, FA, Cs, *etc.*, X = Cl, Br, I) are emerging semiconductor materials, showing the great potentials in the application of light emitting diodes and solar cell devices.[1-8] Besides the development of their device applications, extensive efforts have been made to unravel the fundamental mechanistic origins of their intriguing optoelectronic properties,[9-13] such as long carrier lifetimes and diffusion lengths[14,15] but modest carrier mobilities.[13,16] Concept of polaron formation, in which the photogenerated charge carriers in crystal are localized (or trapped) with the concurrent crystalline structural deformation via strong carrier-phonon interactions, has recently been rationalized to interpret the nature of the outstanding optoelectronic properties of LHPs.[13,17-21] Previous studies using ultrafast THz spectroscopy technique, that is sensitive to intraband correlated motions of charge carriers, revealed direct experimental signatures of polaron states in phtoexcited metal halite perovskites.[22,23] The dynamically screened coulomb potential by polarons reduces the scattering of photoinduced charge carrier by defects, other charge carriers and longitudinal-optical (LO) phonons. The charge carriers transport along the perovskite lattice framework of $[PbX_6]^{4-}$ octahedra (X=Cl, Br or I) are consequently in favor, with lower electron-hole recombination rate. Additionally, polaron formation has been increasingly invoked for theoretically analyzing the *J-V* hysteresis and slow photo-degradation /fast self-healing of devices based on LHPs.[19,24,25] Very recently, first-principle simulations by F. D. Anglis *et al.* revealed that although the polaron formation is mainly within the inorganic framework of $[PbX_6]^{4-}$, it can be affected by A-site cations (e.g. MA, FA, Cs, *etc.*) due to their different polarity and mobility in the cavity of inorganic framework. [26-28] However, the direct experimental proofs are still lacking.

Although the photoexcited charge carrier dynamics of LHPs has been extensively studied by ultrafast optical characterization techniques and their polaron state can be confirmed by THz spectroscopy, it is intrinsically difficult to simultaneous track the electronic and structural evolution of the photoexcited LHPs, which defines the polaron state. Consequently, current experimental studies often lack the clarification on that the polaron state is caused by the localization of electron or hole.[17-19,21,22,24,29-31] The conclusions varying between electron/hole polaron are mainly derived or speculated through simulations based on indirect experimental results. Here, by using the state-of-art, ultrafast synchrotron-based X-ray transient absorption (XTA) spectroscopy (laser pump – X-ray probe, see the setup schematic in Figure S1), we have directly observed the photoexcited electronic and structural change of LHPs, owing to that the XTA technique is intrinsically element-specific, oxidation state and local structure sensitive.[32-34] By employing this technique, we have recently revealed that the photogenerated electron and hole are delocalized and localized (namely, formation of small hole polaron), respectively, within lead-free perovskite nanocrystals.[35] Here we have further measured the more challenging sample system, LHP thin film, mimicking the actual active layer in the device geometry. The direct spectroscopic view of the hole plaron formation in two classic LHP thin films: $MAPbBr_3$ (MA: CH_3NH_3) and $FAPbBr_3$ (FA: $CH(NH_2)_2$) has been revealed by probing at the Br K edge with ps X-ray pulse upon the photoexcitation of fs laser pulse at 530 nm. We have found that at room temperature the photogenerated holes in both LHPs are localized at Br atoms concurrently with local lattice distortion around Br sites, resulting in the hole polaron formation. Interestingly, the LHP containing

the bigger cation FA shows the stronger hole polaron effect, which indicates the slower charge carrier relaxation dyamics.

The 100-nm thick $MAPbBr_3$ and $FAPbBr_3$ thin films on quartz substrates for XTA measurements were fabricated by using a spin-coating method, which is detailed in

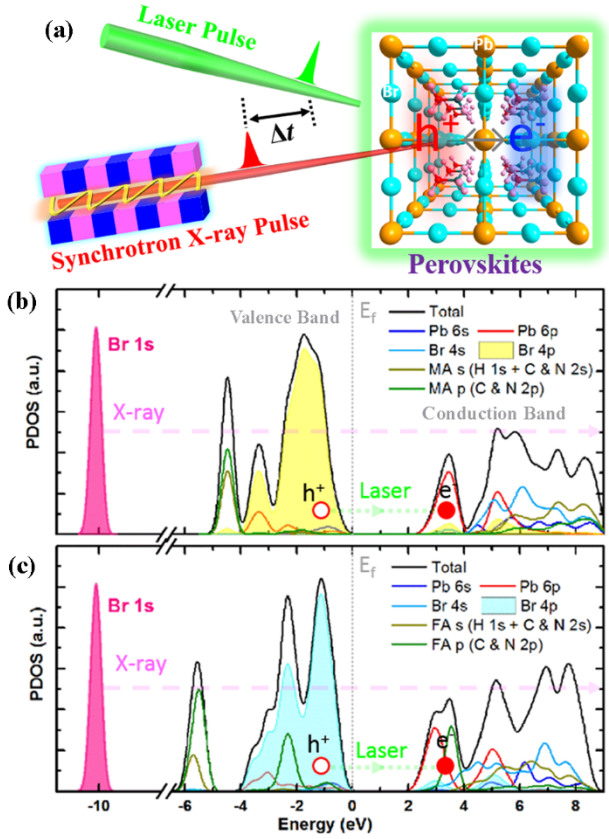

Figure 1. (a) Schematic illustration of XTA measurements (see detailed setup schematic in Figure S1) and DTF-calculated electronic partial density of states (PDOS) of **(b)** MA and **(c)** FA-based perovskites with a cubic phase at room temperature, indicating the atomic orbital compositions of valence and conduction band structures of two systems. In (b) and (c), the Br core 1s orbital is schematic to show the X-ray probe at Br K edge.

the Supporting Information. In order to reduce the sample damage and extend the time of good data collection, the thin film samples were coated with 100-nm PMMA layer. The grazing incidence wide angle X-ray scattering (GIWAXS) measurements identified that both prepared thin films are crystallized very well and they exhibit a cubic phase at room

temperature (Figure S2). Figure S3 shows the steady-state absorption spectra of both samples taken from the transmission measurements, indicating that the absorption exhibits a significant rise near the bandgap due to the contribution of Wannier exciton.[36,37] In regard of the direct optical transition observed in the calculated electronic band structures of LHPs (Figure S4), with Tauc plots of their absorption spectra (Figure S3-Inset), the direct optical band gaps of the prepared MA- and FA-based thin films are determined to 2.31 eV and 2.27 eV, respectively.[38] The XTA characterizations of LHP thin films were performed in a laser pump-X-ray probe configuration (Figure 1a and Figure S1). An ~ 100 fs laser pulse was at first used to initiate the populations of electron (e^-) and hole (h^+) in the samples and then the synchrotron X-ray pulse with FWHM of ~80 ps under Argonne APS 24-bunch operation mode was delivered to monitor the time-dependent electronic and structural evolution of the samples by probing the X-ray absorption at the K edge of Br atoms. The details of our XTA technique including laser and X-ray alignment, data acquisition and process can be found in Supporting Information. Here, to avoid the strong hot carrier thermal effect, the photon energy of the laser pulse (2.34 eV) is chosen to be just a little over the optical energy band gaps of two perovskite samples.

Before running the XTA spectroscopy, which measures the electronic dipole transitions within the specific atom, it is essential to understand the electronic structures of two samples. According to the cubic crystalline phase of MA- and FA-based perovskites at room temperature,[38,39] the band structures of two systems were calculated using DFT method (see Figure S4 in Supporting Information) and they were further projected to generate the electronic partial density of states (PDOS).[39] As shown in

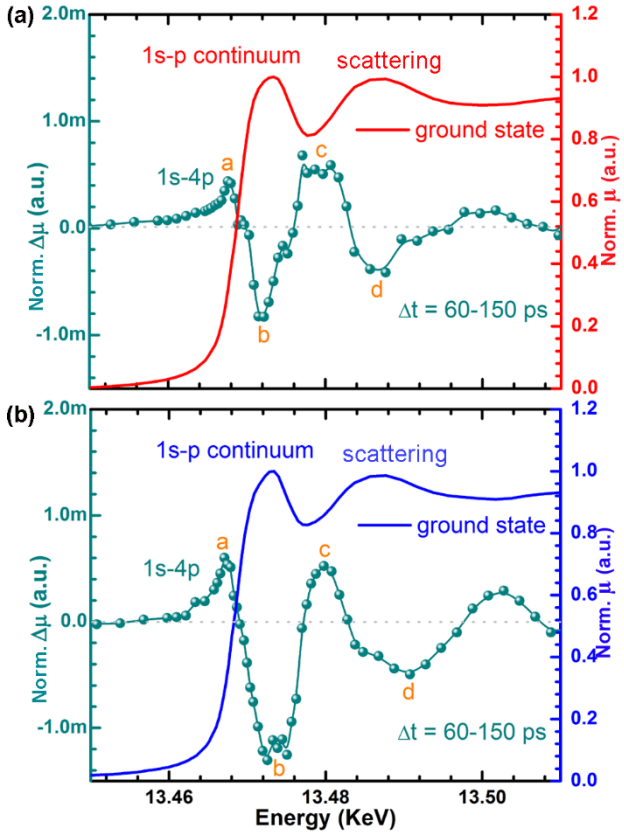

Figure 2. The normalized ground state XA and XTA (Averaged out between Δt = 60-150 ps) spectra of **(a)** MA-based and **(b)** FA-based perovskite thin film samples, measured at Br K edge. The XTA spectra are obtained by the difference between XA spectra with and without laser excitation.

Figure 1b and 1c, the calculated PDOS of two perovskites reveals that the edges of valence band (VB) and conduction band (CB) for two systems are dominated by Br 4p orbital and Pb 6p orbital, respectively. However, the contributions of organic cations to VB and CB are quite different. Compared to the MA p orbitals (combination of C & N p orbitals in MA) nearly completely absent from the VB of MA-based perovskite, FA p orbitals (combination of C & N p orbitals in FA) makes considerate contribution at ~ -2-3 eV (below the Fermi level that is defined at the VB maximum (E_f = 0 eV)). The similar difference also shows in the lower band of CB (~ 2-4 eV above the fermi level). This indicates that FA has stronger interaction with the $[PbX_6]^{4-}$ octahedra than MA via C & N

p orbitals of FA hybridized with Br 4p orbital in VB and Pb 6p orbital in CB. As the laser pulse of 2.34 eV is illuminated on these two systems (Figure 1b and 1c), the electron at the valence band (VB) with primarily Br 4p orbital character can be promoted to the conduction band (CB) of Pb 6p orbital for MA-based perovskite or mixing Pb 6p and FA p orbitals for FA-based perovskite. Since X-ray probing at the Br K edge is to measure the photoexcitation and photoionization of an inner-shell Br 1s electron by X-ray to the Br upper empty and continuum energy-levels with p-orbital characteristics,[40,41] interrogating the Br K edge can unveil the coupled electronic and structural change of two perovskites caused by the photogenerated hole (h^+) due to the laser excitation.

Figure 2 shows the normalized Br K edge X-ray absorption (XA) spectra of two studied thin film samples in the ground state (GS) and the corresponding XTA spectra averaged out between the time-delays Δt = 60-150 ps after the laser excitation. The samples were excited using 2.34 eV photon energy and ~1.4 mJ/cm^2 fluence. The density of absorbed photon numbers are ~7.1 × 10^{14} photons/cm^2 and ~8.97 × 10^{14} photons/cm^2 for MA and FA samples based on their absorbance at 2.34 eV (~0.09 for MA sample and ~0.117 for FA sample; Figure S3 in supporting information). For better comparison of two systems, their XTA spectra (difference between laser-on and laser-off XA spectra) were normalized by the absorbed number of photons. From GS XA spectra in Figure 2a (red) and Figure 2b (blue), we can see that there is an intense edge transition peak at 13.4731 keV, which originates from the allowed dipole electronic transition from Br 1s orbital to p-continuum (called X-ray absorption white line).[40,41] The scattering oscillation peak (13.4864 KeV) above the edge is attributed to the scattering of photoelectron by neighboring atoms of the probed Br atoms, directly reflecting the local geometric lattice

structure around the Br sites.[40,41] Since the XTA spectra were obtained as the difference of XA spectra with and without laser excitation, they can directly deliver the transient electronic and structural change information after photoexcitation. In both Figure 2a and 2b (turquoise), a sharp positive differential absorption peak (a) is apparent in the XTA spectra centered around 13.4673 KeV, arising from a new X-ray absorption transition from Br inner 1s orbital to 4p orbital in VB, where the hole is photocreated by elevating the electron to the CB (Figure 1a and 1b). Once the hole is generated in Br 4p orbital of the VB, the electronic screening for the electron in Br 1s orbital is reduced due to the decreasing electron population in Br 4p orbital. As a result, the photoionization energy of the electron in Br 1s orbital to Br p-continuum increases. This leads to the blue-shift of the white line (Br 1s to p-continuum transition at 13.4731 keV), which produces a negative feature (b) at 13.4731 eV. Therefore, the photoinduced features (a) and (b) here unambiguously demonstrate that the photoexcited holes are localized at Br centers, which agrees with the similar reported observations of the hole trapped at Br 4p orbital in Br_2 molecules[42] and metal bromide nanocrystals.[35,43] The negative spectral feature (d) followed by a small positive peak (13.5025 KeV) due to the blue shift of scattering oscillation peak (13.4864 KeV) also indicates the local lattice structure distortion around Br sites. These fingerprints clearly indicate that the photoinduced hole polaron is formed in these two perovskites. However, compared to MA-based sample, the FA-based one show much larger photoinduced hole polaron effect under exactly same experimental conditions according to the normalized XTA signals.

The hole polaron effect has been experimentally and theoretically studied very well in alkali and alkaline-earth halides,[44-47] where the hole can be easily localized by

moving two adjacent halide ions (X^-) closer to form the X_2^- dimer as hole polaron due to the halide p-orbital characteristics of the valance band. In addition, analogous hole polaron effect has been directly seen in $PbBr_2$ crystal through electron-spin-resonance technique, which exhibits the similar electronic band structure to those of LHPs.[48] Very recently, many theoretical simulations of charge carrier distribution in 3D[19,49-51] and 2D[52-54] LHPs have revealed that a hole localized between two X^- as hole polaron (X_2^-) is more energetically favorable, as compared to that it is delocalized over the whole lattice, and the experimental observation has been further confirmed in 2D metal halide perovskite nanocrystals.[35] Thus, here we propose a similar hole polaron process occurring in the MA- and FA-based perovskite thin films, given their analogous p-orbital featured valance band (Figure 1b and 1c). Due to the intrinsic short-range nature of the X-ray absorption spectroscopy, it only probes averaged local electric and structural information of less than 5-6 Å. Therefore, it is difficult to determine the size of the photoinduced hole polaron by only the XTA. Combining with theoretical calculations will help. However, the corresponding calculation remains challenging due to the uncertain dipole motion of MA and FA cations filled into the $[PbBr_6]^{4-}$ inorganic framework at room temperature[23,53] and the hybridization of FA p orbitals and $[PbBr_6]^{4-}$ electronic states (Figure 1c). This problem might be tackled later with ongoing DFT-based XAS simulations, which are capable of accessing the photoexcited structure of LHPs.

To further understand the different localized hole polaron effect observed in two perovskite thin films , their photoinduced charge-carrier (h^+ and e^-) recombination dynamics were measured by temporally monitoring the photoinduced bleaching recovery of exciton states (2.31 eV for MA and 2.26 eV for FA) due to the state filling in their

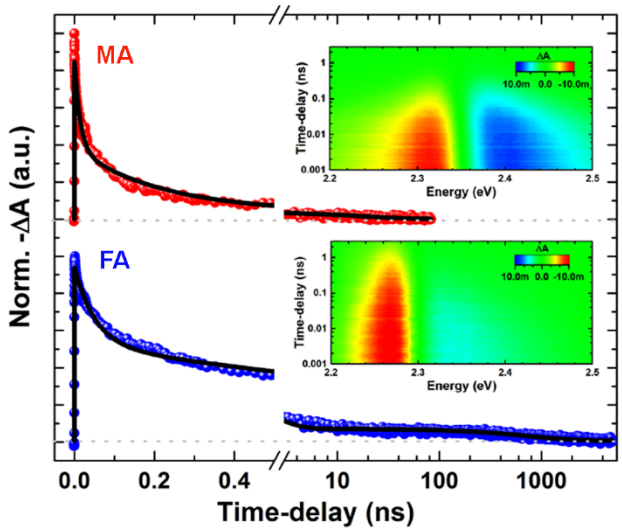

Figure 3. The photoinduced charge-carrier (h^+ and e^-) recombination dynamics of MA- (upper) and FA (bottom) -based samples taken at the exciton photoleaching states (2.31eV for MA and 2.27 eV for FA) showed in the inset pseudocolor images of the OTA spectra. The black cures are three-exponential fits.

optical transient absorption (OTA) spectra. The OTA were measured using 2.75 eV laser photons. To achieve comparable density of absorbed photon numbers, the pump fluence of ~1.3 mJ/cm^2 for MA and ~1.8 mJ/cm^2 for FA was used, to compensate different absorbance at different photon energies in XTA and OTA. (Figure S3 in supporting information).The population of photoexcited chrgcarriers decays much faster in MA-based thin film than that in FA-based one. (Figure 3) The multiple exponential fitting revealed three lifetime components for both perovskite thin films, with those of the MA-perovskite (14 ps (55%), 220 ps (40%) and 18 ns (5%) much shorter than those (51 ps (44%), 1280 ps (49%) and 772 ns (7%)) for the FA-perovskite (Figure 3 bottom). which can be assigned to the Auger recombination, bimolecular radiative recombination and single-molecular recombination (between the electron and localized hole), respectively.[56] Here, the slower relaxation dynamics observed in FA sample can be attributed to the bigger FA cation, p orbitals of which hybridizing into VB and CB (Figure 1c) may favor

the charge separation for enhancing the hole localization at Br center.[26-28,57] As a result, long-lived photoinduced hole localized at Br sites in FA-based thin film exhibits stronger polaron effect. This might be one of intrinsic reasons for the stronger photoluminescence (PL) and longer PL lifetime observed in $FAPbBr_3$ thin film. In fact, by switching the organic cations, the hole localization as a polaron in 2D layered Ruddlesden–Popper perovskite thin films has also been observed in our recent XTA characterizations, which enhances the PL intensity and lifetime.[58]

In summary, by employing XTA spectroscopic technique based on laser pump – X-ray probe, we have investigated the transient electronic and structure properties of 100-nm thick MA- and FA-based LHP thin films upon photoexcitation. The experimental results revealed that the accumulation of long-lived photocreated holes around the optical absorption edge composed of Br 4p orbital is accompanied by distorting local structures around the Br sites. In contrast to the previous studies of the polaron formation in perovskite nanoparticles,[20,33,41] our observations are the direct experimental evidence for confirming the hole polaron formation in solid perovskite thin films, which is expected to help better understand the charge carrier transportation, recombination and trapping as well as the performance of LHP thin films in optoelectronic device applications. In addition, since the atomic orbitals of bigger cation FA strongly hybridize with the electronic states formed by inorganic units $[PbBr_6]^{4-}$, contributing to the VB and CB, the larger hole polaron effect has been discovered in the FA-based LHPs, correlating with the longer charge carrier recombination lifetime. Our study here demonstrated the great potential of using XTA technique to fundamentally understand the photophysical mechanism of charge carriers in LHP based thin film solar cells and LED devices.

Supporting Information

The supporting information is available free of charge on the ACS publication website:

Detailed experimental section including the sample preparation, optical and X-ray transient absorption spectroscopies, and DFT band structure calculations.

Acknowledgments

This work was supported by the U.S. Department of Energy, Office of Science, Office of Basic Energy Sciences under Contract No. DE-AC02-06CH11357. The laser system at 11-ID-D of APS were funded through New Facility and Mid-scale Instrumentation grants to Chemical Sciences and Engineering Division, Argonne National Laboratory (PI: Lin X. Chen). This research used resources of the Advanced Photon Source and the Center for Nanoscale Materials, U.S. Department of Energy (DOE) Office of Science User Facilities operated for the DOE Office of Science by Argonne National Laboratory under Contract No. DE-AC02-06CH11357. This work was performed, in part, at the Center for Integrated Nanotechnologies, an Office of Science User Facility operated for the U.S. Department of Energy (DOE) Office of Science by Los Alamos National Laboratory (Contract 89233218CNA000001).

References

(1) Abdi-Jalebi, M.; Andaji-Garmaroudi, Z.; Cacovich, S.; Stavrakas, C.; Philippe, B.; Richter, J. M.; Alsari, M.; Booker, E. P.; Hutter, E. M.; Pearson, A. J. Maximizing and stabilizing luminescence from halide perovskites with potassium passivation. *Nature* **2018,** *555* (7697), 497.

(2) Lin, K.; Xing, J.; Quan, L. N.; de Arquer, F. P. G.; Gong, X.; Lu, J.; Xie, L.; Zhao, W.; Zhang, D.; Yan, C. Perovskite light-emitting diodes with external quantum efficiency exceeding 20 percent. *Nature* **2018,** *562* (7726), 245.

(3) Nie, W.; Tsai, H.; Asadpour, R.; Blancon, J.-C.; Neukirch, A. J.; Gupta, G.; Crochet, J. J.; Chhowalla, M.; Tretiak, S.; Alam, M. A. High-efficiency solution-processed perovskite solar cells with millimeter-scale grains. *Science* **2015,** *347* (6221), 522-525.
(4) Rong, Y.; Hu, Y.; Mei, A.; Tan, H.; Saidaminov, M. I.; Seok, S. I.; McGehee, M. D.; Sargent, E. H.; Han, H. Challenges for commercializing perovskite solar cells. *Science* **2018,** *361* (6408), eaat8235.
(5) Sahli, F.; Werner, J.; Kamino, B. A.; Bräuninger, M.; Monnard, R.; Paviet-Salomon, B.; Barraud, L.; Ding, L.; Leon, J. J. D.; Sacchetto, D. Fully textured monolithic perovskite/silicon tandem solar cells with 25.2% power conversion efficiency. *Nat. Mater.* **2018,** *17* (9), 820.
(6) Stranks, S. D.; Snaith, H. J. Metal-halide perovskites for photovoltaic and light-emitting devices. *Nat. Nanotechnol.* **2015,** *10* (5), 391.
(7) Turren-Cruz, S.-H.; Hagfeldt, A.; Saliba, M. Methylammonium-free, high-performance, and stable perovskite solar cells on a planar architecture. *Science* **2018,** *362* (6413), 449-453.
(8) Zhu, H.; Fu, Y.; Meng, F.; Wu, X.; Gong, Z.; Ding, Q.; Gustafsson, M. V.; Trinh, M. T.; Jin, S.; Zhu, X. Lead halide perovskite nanowire lasers with low lasing thresholds and high quality factors. *Nat. Mater.* **2015,** *14* (6), 636.
(9) Chen, T.; Chen, W.-L.; Foley, B. J.; Lee, J.; Ruff, J. P.; Ko, J. P.; Brown, C. M.; Harriger, L. W.; Zhang, D.; Park, C. Origin of long lifetime of band-edge charge carriers in organic–inorganic lead iodide perovskites. *Proc. Natl. Acad. Sci.* **2017,** *114* (29), 7519-7524.
(10) Herz, L. M. Charge-carrier dynamics in organic-inorganic metal halide perovskites. *Annu. Rev. Phys.* **2016,** *67*, 65-89.
(11) Herz, L. M. Charge-carrier mobilities in metal halide perovskites: fundamental mechanisms and limits. *ACS Energy Lett.* **2017,** *2* (7), 1539-1548.
(12) Ma, J.; Wang, L.-W. The nature of electron mobility in hybrid perovskite $CH_3NH_3PbI_3$. *Nano Lett.* **2017,** *17* (6), 3646-3654.
(13) Zhu, X.; Podzorov, V. Charge carriers in hybrid organic–inorganic lead halide perovskites might be protected as large polarons. *J. Phys. Chem. Lett.* **2015,** *6* (23), 4758-4761.
(14) Manser, J. S.; Christians, J. A.; Kamat, P. V. Intriguing optoelectronic properties of metal halide perovskites. *Chem. Rev.* **2016,** *116* (21), 12956-13008.
(15) Zhao, D.; Yu, Y.; Wang, C.; Liao, W.; Shrestha, N.; Grice, C. R.; Cimaroli, A. J.; Guan, L.; Ellingson, R. J.; Zhu, K. Low-bandgap mixed tin–lead iodide perovskite absorbers with long carrier lifetimes for all-perovskite tandem solar cells. *Nat. Energy* **2017,** *2* (4), 17018.
(16) Brenner, T. M.; Egger, D. A.; Kronik, L.; Hodes, G.; Cahen, D. Hybrid organic—inorganic perovskites: low-cost semiconductors with intriguing charge-transport properties. *Nat. Rev. Mater.* **2016,** *1* (1), 15007.
(17) Miyata, K.; Atallah, T. L.; Zhu, X.-Y. Lead halide perovskites: Crystal-liquid duality, phonon glass electron crystals, and large polaron formation. *Sci. adv.* **2017,** *3* (10), e1701469.
(18) Miyata, K.; Meggiolaro, D.; Trinh, M. T.; Joshi, P. P.; Mosconi, E.; Jones, S. C.; De Angelis, F.; Zhu, X.-Y. Large polarons in lead halide perovskites. *Sci. adv.* **2017,** *3* (8), e1701217.

(19) Neukirch, A. J.; Nie, W.; Blancon, J.-C.; Appavoo, K.; Tsai, H.; Sfeir, M. Y.; Katan, C.; Pedesseau, L.; Even, J.; Crochet, J. J. Polaron stabilization by cooperative lattice distortion and cation rotations in hybrid perovskite materials. *Nano Lett.* **2016,** *16* (6), 3809-3816.
(20) Zheng, K.; Abdellah, M.; Zhu, Q.; Kong, Q.; Jennings, G.; Kurtz, C. A.; Messing, M. E.; Niu, Y.; Gosztola, D. J.; Al-Marri, M. J. Direct experimental evidence for photoinduced strong-coupling polarons in organolead halide perovskite nanoparticles. *J. Phys. Chem. Lett.* **2016,** *7* (22), 4535-4539.
(21) Zhu, H.; Miyata, K.; Fu, Y.; Wang, J.; Joshi, P. P.; Niesner, D.; Williams, K. W.; Jin, S.; Zhu, X.-Y. Screening in crystalline liquids protects energetic carriers in hybrid perovskites. *Science* **2016,** *353* (6306), 1409-1413.
(22) Cinquanta, E.; Meggiolaro, D.; Motti, S. G.; Gandini, M.; Alcocer, M. J. P.; Akkerman, Q. A.; Vozzi, C.; Manna, L.; Angelis, F. D.; Petrozza, A.; Stagira, S. Ultrafast THz probe of photoinduced polarons in lead-halide perovsites. *Phys. Rev. Lett.* **2019,** *122,* 166601.
(23) Lan, Y.; Dringoli, B. J.; Valverde-Chávez, D. A.; Ponseca Jr. C. S.; Sutton, M.; He, Y.; Kanatzidis, M. G.; Cokke, D. G. Ultrafast correlated charge and lattice motion in a hybrid metail halide perovskites. *Sci. Adv.* **2019,** *5,* eaaw5558.
(24) Nie, W.; Blancon, J.-C.; Neukirch, A. J.; Appavoo, K.; Tsai, H.; Chhowalla, M.; Alam, M. A.; Sfeir, M. Y.; Katan, C.; Even, J. Light-activated photocurrent degradation and self-healing in perovskite solar cells. *Nat. Commun.* **2016,** *7*, 11574.
(25) Zhou, Y.; You, L.; Wang, S.; Ku, Z.; Fan, H.; Schmidt, D.; Rusydi, A.; Chang, L.; Wang, L.; Ren, P. Giant photostriction in organic–inorganic lead halide perovskites. *Nat. Commun.* **2016,** *7*, 11193.
(26) Mahata, A.; Meggiolaro, D.; De Angelis, F. From large to small polarons in lead, tin, and mixed lead–tin halide perovskites. *J. Phys. Chem. Lett.* **2019,** *10* (8), 1790-1798.
(27) Ambrosio, F.; Meggiolaro, D.; Mosconi, E.; De Angelis, F. Charge localization, stabilization, and hopping in lead halide perovskites: Competition between bolaron stabilization and cation disorder. *ACS Energy Lett.* **2019,** *4* (8), 2013-2020.
(28) Meggiolaro, D.; Ambrosio, F.; Mosconi, E.; Mahata, A.; De Angelis, F. Polarons in metal halide perovskites. *Adv. Energy Mater.* **2020,** *10* (13), 1902748.
(29) Ivanovska, T.; Dionigi, C.; Mosconi, E.; De Angelis, F.; Liscio, F.; Morandi, V.; Ruani, G. Long-lived photoinduced polarons in organohalide perovskites. *J. Phys. Chem. Lett.* **2017,** *8* (13), 3081-3086.
(30) Motta, C.; Sanvito, S. Electron–phonon coupling and polaron mobility in hybrid perovskites from first principles. *J. Phys. Chem. C* **2018,** *122* (2), 1361-1366.
(31) Park, M.; Neukirch, A. J.; Reyes-Lillo, S. E.; Lai, M.; Ellis, S. R.; Dietze, D.; Neaton, J. B.; Yang, P.; Tretiak, S.; Mathies, R. A. Excited-state vibrational dynamics toward the polaron in methylammonium lead iodide perovskite. *Nat. Commun.* **2018,** *9* (1), 2525.
(32) Chen, L. X.; Zhang, X. Photochemical processes revealed by X-ray transient absorption spectroscopy. *J. Phys. Chem. Lett.* **2013,** *4* (22), 4000-4013.
(33) Chen, L. X.; Zhang, X.; Shelby, M. Recent advances on ultrafast X-ray spectroscopy in the chemical sciences. *Chem. Sci.* **2014,** *5* (11), 4136-4152.
(34) Liu, C.; Zhang, J.; Lawson Daku, L. v. M.; Gosztola, D.; Canton, S. E.; Zhang, X. Probing the impact of solvation on photoexcited spin crossover complexes with high-

precision x-ray transient absorption spectroscopy. *J. Am. Chem. Soc.* **2017,** *139* (48), 17518-17524.
(35) Liu, C.; Wang, Y.; Geng, H.; Zhu, T.; Ertekin, E.; Gosztola, D.; Yang, S.; Huang, J.; Yang, B.; Han, K. Asynchronous photoexcited electronic and structural relaxation in lead-free perovskites. *J. Am. Chem. Soc* **2019,** *141* (33), 13074-13080.
(36) Elliott, R. Intensity of optical absorption by excitons. *Phys. Rev.* **1957,** *108* (6), 1384.
(37) Saba, M.; Cadelano, M.; Marongiu, D.; Chen, F.; Sarritzu, V.; Sestu, N.; Figus, C.; Aresti, M.; Piras, R.; Lehmann, A. G. Correlated electron–hole plasma in organometal perovskites. *Nat. Commun.* **2014,** *5*, 5049.
(38) Hanusch, F. C.; Wiesenmayer, E.; Mankel, E.; Binek, A.; Angloher, P.; Fraunhofer, C.; Giesbrecht, N.; Feckl, J. M.; Jaegermann, W.; Johrendt, D. Efficient planar heterojunction perovskite solar cells based on formamidinium lead bromide. *J. Phys. Chem. Lett.* **2014,** *5* (16), 2791-2795.
(39) Jacobsson, T. J.; Correa-Baena, J.-P.; Pazoki, M.; Saliba, M.; Schenk, K.; Grätzel, M.; Hagfeldt, A. Exploration of the compositional space for mixed lead halogen perovskites for high efficiency solar cells. *Energ. Environ. Sci.* **2016,** *9* (5), 1706-1724.
(40) Uno, K.; Notoya, Y.; Fujikawa, T.; Yoshikawa, H.; Nishikawa, K. Br K-edge X-ray absorption near edge structure analyses of bromine residue carbon compounds using full multiple-scattering theory. *Jpn. J. Appl. Phys.* **2005,** *44* (6R), 4073.
(41) Morawitz, H.; Bagus, P.; Clarke, T.; Gill, W.; Grant, P.; Street, G. B. X-ray Absorption in Polymers. *Synth. Met.* **1979/80,** *1*, 267-278.
(42) Elles, C. G.; Shkrob, I. A.; Crowell, R. A.; Arms, D. A.; Landahl, E. C. Transient x-ray absorption spectroscopy of hydrated halogen atom. *J. Chem. Phys.* **2008,** *128*, 061102.
(43) Santomauro, F.; Rossi, T.; Budarz, J.; Kovalenko, M. V.; Mewes, L.; Samson, V.; Smolentsev, G.; Kinschel, D.; Nedelcu, G.; Capano, G. Localized holes and delocalized electrons in photoexcited inorganic perovskites. *Struct. Dyn.* **2017,** *4*, 044002.
(44) Beaumont, J.; Hayes, W.; Kirk, D.; Summers, G. An investigation of trapped holes and trapped excitons in alkaline earth fluorides. *Proc. R. Soc. Lond. A* **1970,** *315* (1520), 69-97.
(45) Crawford Jr., J. H.; Slifkin, L. M. *Points defects in solids*. Springer Boston, 1972.
(46) Hayes, W.; Twidell, J. The self-trapped hole in CaF_2. *Proc. Phys. Soc.* **1962,** *79* (6), 1295.
(47) Castner, T. G.; Känzig, W. The electronic structure of V-centers. *J. Phys. Chem. Solids* **1957,** *3* (3-4), 178-195.
(48) Iwanaga, M.; Azuma, J.; Shirai, M.; Tanaka, K.; Hayashi, T. Self-trapped electrons and holes in $PbBr_2$ crystals. *Phy. Rev. B* **2002,** *65* (21), 214306.
(49) Peng, C.; Wang, J.; Wang, H.; Hu, P. Unique trapped dimer state of the photogenerated Hole in hybrid orthorhombic $CH_3NH_3PbI_3$ perovskite: Identification, origin, and implications. *Nano Lett.* **2017,** *17* (12), 7724-7730.
(50) Kang, B.; Biswas, K. Shallow trapping vs. deep polarons in a hybrid lead halide perovskite, $CH_3NH_3PbI_3$. *Phys. Chem. Chem. Phys.* **2017,** *19* (40), 27184-27190.
(51) Whalley, L. D.; Crespo-Otero, R.; Walsh, A. H-center and V-center defects in hybrid halide perovskites. *ACS Energy Lett.* **2017,** *2* (12), 2713-2714.
(52) Cortecchia, D.; Yin, J.; Bruno, A.; Lo, S.-Z. A.; Gurzadyan, G. G.; Mhaisalkar, S.; Brédas, J.-L.; Soci, C. Polaron self-localization in white-light emitting hybrid perovskites. *J. Mater. Chem. C* **2017,** *5* (11), 2771-2780.

(53) Smith, M. D.; Karunadasa, H. I. White-light emission from layered halide perovskites. *Acc. Chem. Res* **2018,** *51* (3), 619-627.
(54) Yin, J.; Li, H.; Cortecchia, D.; Soci, C.; Brédas, J.-L. Excitonic and polaronic properties of 2D hybrid organic–inorganic perovskites. *ACS Energy Lett.* **2017,** *2* (2), 417-423.
(55) Huang, X.; Sendner, M.; Müller, C.; Sessolo, M.; Gil-Escrig, L.; Kowalsky, W.; Pucci, A.; Beck, S.; Lovrinčić, R. Quantifying the Composition of Methylammonium Lead Iodide Perovskite Thin Films with Infrared Spectroscopy. *J. Phys. Chem. C* **2019,** *123* (36), 22083-22088.
(56) Zheng, K.; Žídek, K.; Abdellah, M.; Chen, J.; Cháhera, P.; Zhang, W.; Al-Marri, M. J.; Pullerits, T. High excitation intensity opens a new trapping channel in orgnaic-inorganic hybrid perovskite nanoparticles. *ACS Energy Lett.* **2016,** 1 (6), 1154-1161.
(57) Frost, J. M.; Butler, K. T.; Brivio, F.; Hendon, C. H.; Van Schilfgaarde, M.; Walsh, A. Atomistic origins of high-performance in hybrid halide perovskite solar cells. *Nano Lett.* **2014,** *14* (5), 2584-2590.
(58) Tsai, H.; Liu, C.; Kinigstein, E.; Li, M.; Tretiak, S.; Cotlet, M.; Ma, X.; Zhang, X.; Nie, W. Critical role of organic spacers for bright 2D layered perovskites light-emitting diodes. *Adv. Sci.* **2020**, 1903202.